NUMERICAL STUDY OF THE THERMAL EFFECTS INDUCED BY A RFID ANTENNA IN VIALS OF BLOOD PLASMA

R. Otin

CIMNE —
International Center for Numerical Methods in Engineering
Parque Mediterráneo de la Tecnología (PMT)
Av. del Canal Olímpico, s/n-Edificio C3-Despacho 206
Castelldefels, Barcelona 08860, Spain

Abstract—This paper presents a numerical study of the thermal effects induced by a commercial RFID antenna in vials filled with blood plasma. The antenna is located under a conveyor belt which transports cardboard boxes bearing test tubes or pooling bottles. Part of the energy used to read the RFID tags penetrates into the vials and heats the plasma. Our aim is to assess if the RFID technology can alter the quality of the blood plasma by increasing excessively its temperature. To do so, we first compute the specific absorption rate inside the vials with the finite element method. Then, assuming that no heat dissipation process is present, we estimate the number of continuous reading cycles required to increase the plasma temperature $0.1\,^\circ\text{C}$ in the worst-case scenario.

1. INTRODUCTION

RFID stands for Radio Frequency IDentification, and it consists in the use of a tag incorporated into a product, animal, or person for the purpose of identification using radio waves. There are basically two types of RFID tags: active tags, which can transmit signals autonomously, and passive tags, which require an external energy source to transmit signals. The RFID process of passive tags, which is the case of interest here, is as follows. First, the tag receives electromagnetic energy from the RFID reader. Then, the tag uses this energy to send back the data stored in it. Finally, the reader

receives the tag's radio waves and interprets the signals. A collateral effect of the reading process is that part of the energy radiated by the RFID antenna penetrates into the object where the tag is incorporated and heats it. The aim of this work is to study numerically the induced heating and assess if the RFID technology can alter the properties of the blood plasma by increasing excessively its temperature.

2. DESCRIPTION OF THE PROBLEM

Cardboard boxes bearing test tubes (or pooling bottles) filled with blood plasma are moved along a conveyor belt which has a RFID antenna beneath it. When the boxes pass above the antenna, it reads the passive RFID tags incorporated into the vials. Some of the electromagnetic radiation used to read the tags is absorbed by the blood plasma contained in the vials. The absorbed radiation heats the blood plasma and increases its temperature. The question we try to answer in this study is how fast the temperature increases in the worst-case scenario. More specifically, we calculate the time required to increase the temperature $0.1\,^\circ$C, at the point of maximum radiation absorption, and under the supposition that no mechanism of heat dissipation is acting during the excitation. Once this is known, we can determine the number of continuous reading cycles needed to produce such a temperature increase and if this number is much higher or lower than the number of reading cycles required to obtain all the data from the tags under normal usage conditions.

Although there exist several studies and strict regulations regarding human exposure to RFID antennas (see for instance [1, 10]), it does not happen the same with the effects of the radiation on the products in where the RFID tags are attached. In fact, we have found only one previous work pursuing this objective [2], which evaluates the effects of a RFID antenna on vials of insulin. Then, to assess if a RFID system is safe for the blood plasma, we fixed the criterium detailed above.

The heating induced by the RFID antenna was computed for blood plasma at room temperature ($+25\,^\circ$C) and frozen ($-30\,^\circ$C). The physical properties of the blood plasma at both temperatures are summarized in Table 1. The plasma is carried in test tubes or pooling bottles which are inside cardboard boxes containing 96 test tubes or 15 pooling bottles (see Figure 1). The cardboard boxes are transported by a conveyor belt passing above the RFID antenna. The commercial RFID antenna used for tag identification is a CS-777 Bricyard operating at a frequency of $f = 915\,$MHz and with an input power of $P_0 = 1\,$W.

Table 1. Physical properties of the blood plasma at room temperature $(+25\,°\text{C})$ and frozen $(-30\,°\text{C})$, being ϵ_r' the real part of the relative electric permittivity, ϵ_r'' the imaginary part of the relative electric permittivity, ϵ_0 the vacuum permittivity, σ the electrical conductivity, ρ the mass density and c the specific heat capacity at constant pressure. Data extrapolated from [4–7].

T (°C)	$\epsilon_r'(\epsilon'/\epsilon_0)$	$\epsilon_r''(\epsilon''/\epsilon_0)$	σ (S/m)	ρ (Kg/m^3)	c (J/Kg°C)
$+25$	70	0	1.7	1025	3780
-30	3	0.3	0	920	2050
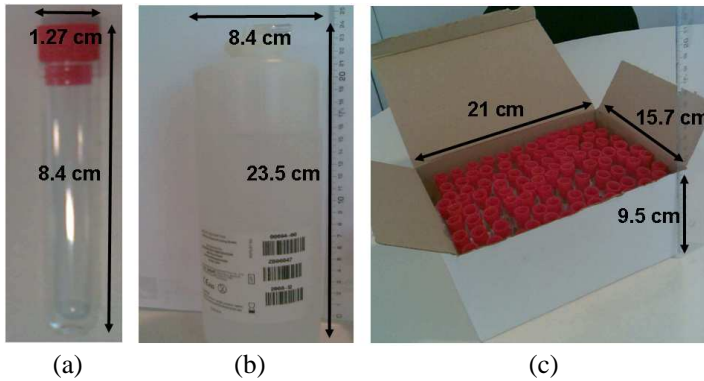
Figure 1. (a) Dimensions of a test tube. (b) Dimensions of a pooling bottle. (c) Dimensions of the cardboard box containing 96 test tubes. A similar box is used to transport 15 pooling bottles.

3. NUMERICAL MODEL

This section presents the mathematical model used to calculate the thermal heating induced by the RFID antenna in the vials of blood plasma. In Subsection 3.1, we describe the finite element formulation employed for computing the electric field generated by the antenna. In Subsection 3.2, we give the expressions relating the electric field with the thermal heating as the temperature increase.

3.1. Finite Element Model

To compute the electric field we used the in-house code ERMES (Electric Regularized Maxwell Equations with Singularities). This code is the C++ implementation of the finite element formulation

showed in [8]. When applied to the problem discussed here, this formulation consists in finding $\mathbf{E} \in \mathbf{H}_0(\mathbf{curl}, \mathrm{div}; \Omega)$ such that $\forall \mathbf{F} \in \mathbf{H}_0(\mathbf{curl}, \mathrm{div}; \Omega)$ holds

$$\int_\Omega \frac{1}{\mu}(\nabla \times \mathbf{E}) \cdot (\nabla \times \bar{\mathbf{F}}) + \int_\Omega \frac{1}{\mu \varepsilon \bar{\varepsilon}}(\nabla \cdot (\varepsilon \mathbf{E})) \cdot (\nabla \cdot (\bar{\varepsilon}\bar{\mathbf{F}}))$$

$$-\omega^2 \int_\Omega \varepsilon(\mathbf{E} \cdot \bar{\mathbf{F}}) - i\omega\sqrt{\frac{\epsilon_0}{\mu_0}} \int_{\partial\Omega_r}(\mathbf{E} \cdot \bar{\mathbf{F}}) = i\omega \int_\Omega \mathbf{J} \cdot \bar{\mathbf{F}}, \qquad (1)$$

where Ω is the problem domain, $\partial\Omega_r$ is the surface where the first order absorbing boundary condition (1st ABC) is applied, $\mathbf{E}$ is the electric field, ω is the angular frequency, $\mathbf{J}$ is the current density, μ is the magnetic permeability and $\varepsilon = \epsilon' + i(\epsilon'' + \sigma/\omega)$ is the complex electric permittivity. The bar over the magnitudes denotes the complex conjugate. The functional space $\mathbf{H}_0(\mathbf{curl}, \mathrm{div}; \Omega)$ is defined by

$$\mathbf{H}_0(\mathbf{curl}, \mathrm{div}; \Omega) : = \{\mathbf{F} \in \mathbf{L}^2(\Omega) | \nabla \times \mathbf{F} \in \mathbf{L}^2(\Omega), \nabla \cdot (\varepsilon\mathbf{F}) \in L^2(\Omega),$$
$$\hat{\mathbf{n}} \times \mathbf{F} = 0 \text{ in PEC}, \ \hat{\mathbf{n}} \cdot \mathbf{F} = 0 \text{ in PMC}\}. \qquad (2)$$

A perfect electric conductor (PEC) boundary is where we apply the conditions

$$\nabla \cdot (\varepsilon\mathbf{E}) = 0,$$
$$\hat{\mathbf{n}} \times \mathbf{E} = 0. \qquad (3)$$

A perfect magnetic conductor (PMC) boundary is where we apply the condition

$$\hat{\mathbf{n}} \times \nabla \times \mathbf{E} = 0,$$
$$\hat{\mathbf{n}} \cdot \mathbf{E} = 0. \qquad (4)$$

The first order absorbing boundary condition (1st ABC) is expressed in this formulation as

$$\hat{\mathbf{n}} \times \nabla \times \mathbf{E} = i\omega\sqrt{\epsilon_0\mu_0}(\hat{\mathbf{n}} \times \hat{\mathbf{n}} \times \mathbf{E}),$$
$$\nabla \cdot \mathbf{E} = i\omega\sqrt{\epsilon_0\mu_0}(\hat{\mathbf{n}} \cdot \mathbf{E}), \qquad (5)$$

where μ_0 is the vacuum permeability. In Figure 2 is shown the finite element model used in this study. We applied the PEC boundary condition (3) to the ground, the first order absorbing boundary condition (5) to the exterior surface and the PMC boundary condition (4) to the symmetry planes. In the surfaces of discontinuity between two media, we apply the double-node technique explained in [8].

In Figure 2 is shown a quarter of the cardboard box containing 96 test tubes and a quarter of the cardboard box containing 15 poling bottles. The dimensions of the test tubes box are detailed in Figure 1. Inside this box there are 8 rows of 12 test tubes. The distance between
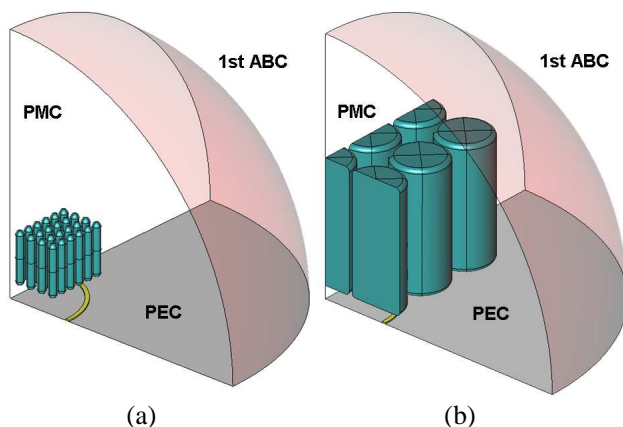
Figure 2. (a) FEM model of the cardboard box containing 96 test tubes. (b) FEM model of the cardboard box containing 15 pooling bottles.

tubes in the same row is 0.24 cm. The distance between rows of test tubes is 0.35 cm. Inside the pooling bottle box there are 3 rows of 5 plasma pooling bottles. The distance between bottles in the same row is 0.5 cm. The distance between the rows of bottles is also 0.5 cm. The boxes are positioned just above the RFID antenna.

The antenna CS-777 Bricyard is a segmented loop antenna [3, 9] designed for UHF near-field RFID applications. This type of antenna produce a strong and uniform magnetic field distribution in the near-field region, which ensures a good inductive coupling between the tag and the antenna. Such a coupling system is the most appropriate to operate in the vicinity of liquids and metals with low magnetic permeability. The characteristic field distribution of a segmented loop antenna is achieved with an electrical current which is in-phase and has the same magnitude along the loop. Therefore, we have modeled the CS-777 Bricyard as a circular current loop of constant phase and magnitude. The loop has an internal diameter of 20 cm and a rectangular section which is 0.6 cm wide and 0.2 cm high. The current loop is enclosed in a metallic case with a plastic cover in the front. To model the casing of the antenna, we placed the current loop on a PEC plane separated 2 cm from the bottom of the cardboard boxes. We impose a radiated output power of $P_0 = 1$ W by multiplying the computed $\mathbf{E}$ field by the constant

$$\alpha = \sqrt{\frac{2P_0}{-\int_s Real[\mathbf{E} \cdot \bar{\mathbf{J}}]}},\qquad(6)$$

where s is the volume of the current loop. We multiply the fields by α to impose that all the power sent to antenna is radiated, which is the worst-case scenario.

To solve numerically the functional problem (1)–(5), ERMES employed about 8e5-1e6 tetrahedral second order nodal elements. The resulting liner systems had around 3e6-4e6 unknowns and the RAM memory required was about 6–7 GB. The time needed to reach a residual ($\|Ax - b\|/\|b\|$) of less than 1e-4 was about 2–3 hours with a non-parallel quasi-minimal residual (QMR) iterative solver and a diagonal preconditioner. These data are referred to a desktop computer with a CPU Intel Core 2 Quad Q9300 at 2.5 GHz and the operative system Microsoft Windows XP Professional x64 Edition v2003.

3.2. Thermal Heating

The specific absorption rate (SAR) relates the electric field computed above with the thermal heating. The SAR is defined as

$$\text{SAR (W/kg)} = \frac{\sigma + \omega\epsilon''}{2\rho}|\mathbf{E}|^2 \tag{7}$$

where σ is the electrical conductivity, ϵ'' is the imaginary part of the electric permittivity, ω is the frequency, ρ is the mass density and $\mathbf{E}$ is the electric field. This expression represents the time-average power per unit mass dissipated as heat due to conductivity and dielectric losses.

The relation of the SAR with the temperature can be very complex if we take into account heat dissipation processes such as conduction or convection. However, if we want to calculate the temperature increase in the worst-case scenario, where all the electromagnetic energy is used to increase temperature and any mechanism of heat dissipation is present, this relation is very simple,

$$\Delta T \approx \frac{\text{SAR}\Delta t}{c}, \tag{8}$$

where ΔT is the temperature increase, c is the specific heat capacity and Δt is the duration of the electromagnetic excitation.

4. RESULTS

The results of the simulations are shown in Figures 3, 4, 5, 6, 7 and 8. We see that the higher SAR is found in the vials positioned just atop the current loop of the antenna. The values of the maximum SAR (SAR_{max}) obtained in each case are summarized in Table 2. Once the SAR is known, we calculate with Equation (8) the time (Δt) needed
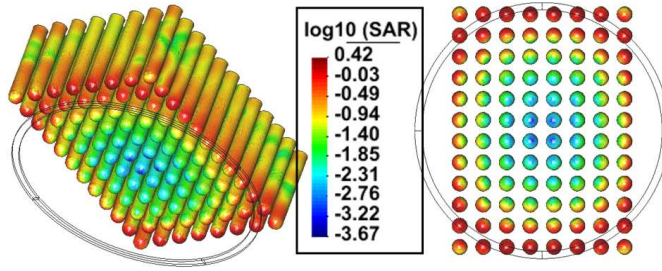
Figure 3. SAR distribution in the box containing 96 test tubes with blood plasma at room temperature ($+25\,°$C). Logarithmic scale.
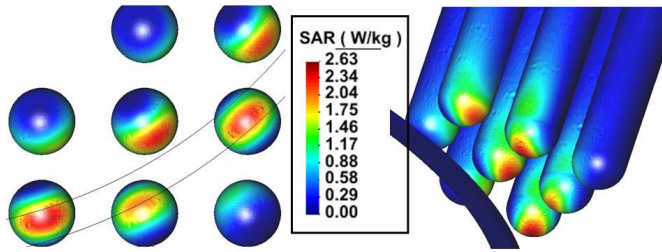
Figure 4. SAR distribution in the box containing 96 test tubes with blood plasma at room temperature ($+25\,°$C). Detail.
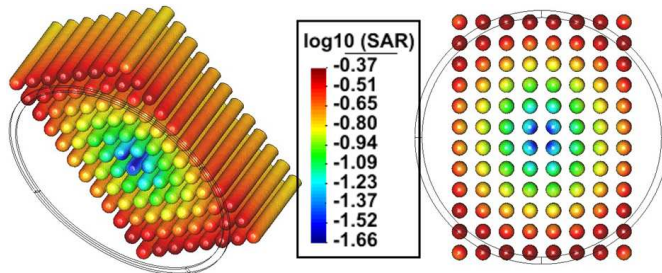
Figure 5. SAR distribution in the box containing 96 test tubes with frozen blood plasma ($-30\,°$C). Logarithmic scale.

to increase the temperature of the blood plasma $\Delta T = 0.1\,°$C, at the point of maximum SAR, and assuming that no mechanism of heat dissipation is present (see Table 3).
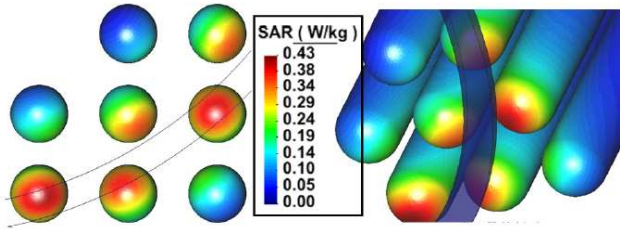
Figure 6. SAR distribution in the box containing 96 test tubes with frozen blood plasma ($-30\,°\mathrm{C}$). Detail.
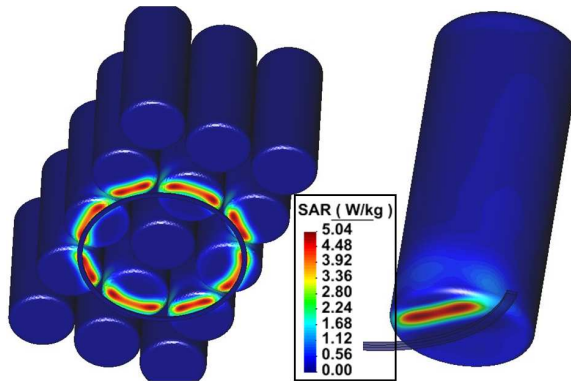
Figure 7. SAR distribution in the box containing 15 pooling bottles with blood plasma at room temperature ($+25\,°\mathrm{C}$).
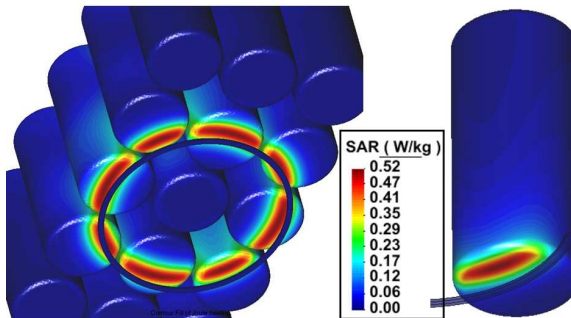
Figure 8. SAR distribution in the box containing 15 pooling bottles with frozen blood plasma ($-30\,°\mathrm{C}$).

Table 2. Maximum SAR (SAR$_{max}$).

T (°C)	Test tube SAR$_{max}$ (W/Kg)	Pooling bottle SAR$_{max}$ (W/Kg)
+25	2.63	5.04
−30	0.43	0.52

Table 3. Time (Δt) needed to increase the temperature of the blood plasma $\Delta T = 0.1$ °C, at the point of maximum SAR, and assuming that no mechanism of heat dissipation is present.

T (°C)	Test tube Δt (s)	Pooling bottle Δt (s)
+25	144	75
−30	477	394

5. CONCLUSIONS

As can be seen in the Table 3, the shorter time is $\Delta t = 75$ s for the pooling bottle at room temperature (+25 °C). Then, since a typical read cycle lasts 100 ms, it would take 750 continuous reading cycles to produce an increase 0.1 °C, at the point of maximum radiation absorption, and without any mechanism of heat dissipation present. So, we can conclude that, the RFID technology analyzed in this work do not alter the quality of the blood plasma in a standard situation of a few readings cycles, with the vials being carried by a conveyor belt equipped with RFID antennas. The only scenario that would present a problem would be a box left forgotten just above a RFID reader in continuous operation. However, this situation is very unlikely because motion detectors are usually placed in the conveyor belt and the RFID readers are only activated when the belt is moving.

REFERENCES

1. Arumugam, D. D. and D. W. Engels, "Specific absorption rates in the human head and shoulder for passive UHF RFID systems," *Int. J. Radio Frequency Identification Technology and Applications*, Vol. 2, Nos. 1–2, 1–26, 2009.

2. Bassen, H., "Liquid pharmaceuticals and 915 MHz radiofrequency identification systems, worst-case heating and induced electric fields," *RFID Journal*, http://www.rfidjournal.com/whitepapers/7/3, Sep. 2005.

3. Dobkin, D. M., S. M. Weigand, and N. Iye, "Segmented magnetic antennas for near-field UHF RFID," *Micro. J.*, Vol. 50, No. 6, 2007.

4. Federal Communications Commission (FCC), "Body tissue dielectric parameters," http://www.fcc.gov/oet/rfsafety/dielectric.html, 2010.

5. Hinhofer-Szalkay, H., "Method of high-precision microsample blood and plasma mass densiometry," *J. Appl. Physiol.*, Vol. 60, No. 3, 1082–1088, 1986.

6. Jaspard, F., M. Nadi, and A. Rouane, "Dielectric properties of blood: An investigation of haematocrit dependence," *Physiol. Meas.*, Vol. 24, No. 1, 137–147, 2003.

7. Kashyap, S. C., "Dielectric properties of blood plasma," *Electron. Lett.*, Vol. 17, No. 19, 713–714, 1981.

8. Otin, R., "Regularized Maxwell equations and nodal finite elements for electromagnetic field computations," *Electromagnetics*, Vol. 30, Nos. 1–2, 190–204, 2010.

9. Qing, X., C. K. Goh, and Z. N. Chen, "Segmented loop antenna for UHF near-field RFID applications," *Electron. Lett.*, Vol. 45, No. 7, 872–873, 2009.

10. Sanchis, A., J. Espinosa-García, and A. Martín, "Numerical simulation of EM environment and human exposure when using RFID devices," *PIERS Online*, Vol. 6, No. 7, 651–654, 2010.